

A General Pressure Gradient Formulation for Ocean Models

Part I: Scheme Design and Diagnostic Analysis

Y. Tony Song

Earth and Space Sciences Division

Jet Propulsion Laboratory

California Institute of Technology

Pasadena, CA 91109

song@pacific.JPL.NASA.GOV

Submitted to the *Monthly Weather Review* (Revised)

February 18, 1998

Abstract

A Jacobian formulation of the pressure gradient force for use in models with topography-following coordinates is proposed. It can be used in conjunction with any vertical coordinate system and is easily implemented. Vertical variations in the pressure gradient are expressed in terms of a vertical integral of the Jacobian of density and depth with respect to the vertical computational coordinate. Finite difference approximations are made on the density field, consistent with piecewise linear and continuous fields, and accurate pressure gradients are obtained by vertical integrating the discrete Jacobian from sea surface.

Two discrete schemes are derived and examined in detail: the first using standard centered differencing in the generalized vertical coordinate and the second using a vertical weighting such that the finite differences are centered with respect to the Cartesian z coordinate. Both schemes achieve second order accuracy for any vertical coordinate system and are significantly more accurate than conventional schemes based on estimating the pressure gradients by finite differencing a previously determined pressure field.

The standard Jacobian formulation is constructed to give exact pressure gradient results, independent of the bottom topography, if the buoyancy field varies bilinearly with horizontal position, x , and the generalized vertical coordinate, s , over each grid cell. Similarly, the weighted Jacobian scheme is designed to achieve exact results, when the buoyancy field varies bilinearly with x and z over each grid cell.

When horizontal resolution cannot be made fine enough to avoid hydrostatic inconsistency, errors can be substantially reduced by the choice of an appropriate vertical coordinate. Tests with horizontally uniform, vertically varying, and with horizontally and vertically varying buoyancy fields show that the standard Jacobian formulation achieves superior results when the condition for hydrostatic consistency is satisfied, but when coarse horizontal resolution causes this condition to be strongly violated, the weighted Jacobian may give superior results.

1 Introduction

Topography-following coordinate systems are gaining popularity in numerical models because they simplify aspects of the computations by mapping the varying topography into a regular domain, and they can be used to better resolve the surface and bottom layers of the ocean. For these reasons, the sigma (σ) coordinate system, which is the linear function of bottom topography proposed by Phillips (1957) (see Appendix A), is now used widely in both atmospheric and oceanic modeling.

Several generalized topography-following coordinate systems have recently been proposed for improving resolution in the surface and bottom boundary layers of ocean models. Examples include the hybrid coordinate of Gerdes (1993) and the s -coordinate of Song and Haidvogel (1994). Numerous ocean circulation models have been developed based on topography-following coordinates, including the Princeton Ocean Model (POM, Blumberg and Mellor 1987), the Lamont-Doherty Ocean-Atmosphere Model (LOAM, Zebiak and Cane 1987), and the S -Coordinate Rutgers University Model (SCRUM, Song and Haidvogel 1994). Applications have been made to a broad range of oceanographic problems, including estuarine, coastal and large-scale ocean circulation problems (e.g., Oey et al. 1985; Glenn et al. 1996; Spall and Robinson 1990; Mellor and Ezer 1991).

Unfortunately, models using topography-following coordinates have suffered from errors in the horizontal components of the pressure gradient over steep topography. The source of this error is easily understood. For example, in σ coordinates, the x -component of the pressure gradient force is determined by the sum of two terms, i.e.,

$$\left. \frac{\partial p}{\partial x} \right)_z = \frac{\partial p}{\partial x} - \frac{\sigma}{h} \frac{\partial p}{\partial \sigma} \frac{\partial h}{\partial x}, \quad (1.1)$$

where $\sigma \equiv z/h$. The first term on the right involves the variation of pressure along a constant σ -surface and the second involves the usual vertical variation of pressure. Near steep topography these terms are large, comparable in magnitude, and typically opposite in sign. In such cases, a small error in computing either term can result in a large error in the total horizontal pressure gradient force. This problem was first realized by Smagorinsky et al. (1967).

Later, Janjic (1977) and Mesinger (1981) pointed out an undesirable feature of the pressure gradient calculation in σ -coordinates which is often referred as “hydrostatic inconsistency” (see section 3.1 for further discussion). More recently, Haney (1991) has focused the attention of the ocean modeling community on the pressure gradient error associated with the use of topography-following coordinates.

Steep topography plays an important role in ocean dynamics and particular care is required to reduce the possibility of serious errors when using topography-following coordinates in numerical models. Over the past three decades, meteorologists and oceanographers have put a great deal of effort into the development of accurate and efficient numerical methods for use in such models. These efforts can be divided into the following four categories.

1) Vertical interpolation method:

This is a method of interpolating density back to z -levels to calculate the pressure gradient force. Special care is required to avoid numerical errors which can cause serious problems since integral properties are not guaranteed. One particular problem is that extrapolation is often required when dealing with the highest and lowest levels of the model over steep topography. In addition, this method would be very costly if the interpolation were required at every time step and every grid point, particularly if the σ -levels were allowed to be time dependent as in free surface models. Discussion of this method can be found in Mahrer (1984) and Fortunato and Baptista (1996).

2) Subtract reference state:

Another technique is to formulate the pressure gradient force in terms of deviations from a suitably chosen reference state $\bar{\rho}(z)$ (Gary, 1973). This technique is simple to implement and has proven useful in limited area ocean models, where the departure of the density from the reference state is relatively small. However, it may be of less help in large-scale models or in long-time integrations where the departures may not be small. References to other papers discussing this method can be found in Corby et al. (1972) and Batteen (1988).

3) Higher order methods:

The use of higher order numerical schemes to estimate the pressure gradient term has also been proposed to minimize errors. Beckmann and Haidvogel (1993) use the spectral method and correct for truncation errors based on a Taylor series expansion of z -base functions, and McCalpin (1992) introduces a fourth-order approximation for the horizontal derivatives of pressure along σ -levels (the first term on the right side of equation (1.1)). Such high order methods should yield a more accurate pressure gradient force. However, this approach fails to achieve significant improvement in some cases, such as the case of strongly stratified flow reported by Beckmann and Haidvogel (1993).

4) Retaining integral properties:

Arakawa and Suarez (1983) and Arakawa and Konor (1996) emphasize the requirement for the discrete formulation to retain important integral properties of the continuous equations. Since errors in the discrete equations cannot be eliminated completely, certain integral properties should be satisfied to avoid the gradual development of large errors, perhaps due to spurious sources and/or sinks of total mass, energy or vorticity. Based on the formulation (1.1), they design some discrete schemes which conserve a variety of important integral properties. Clearly, the best pressure gradient formulation should minimize truncation errors while simultaneously retaining important integral properties.

From this brief review of the work associated with the σ -coordinate system, it is clear that there is great concern about the pressure gradient formulation. As more generalized vertical coordinate models are developed (e.g., Zhu et al, 1992; Gerdes, 1993; Song and Haidvogel, 1994; Arakawa and Konor, 1996), two questions must be addressed: (1) Is there a generalized pressure gradient formulation which is suitable for all such models, and (2) How well does any particular formulation deal with the interaction of buoyancy variations and steep topography?

The primary goal of this study is to introduce a pressure gradient formulation which is suitable for use with generalized topography-following coordinate systems. So far, most efforts to improve the pressure gradient formulation have been based on (1.1) or similar expressions where the gradient is applied after the pressure has been determined on σ -surfaces. One

example is the Arakawa and Suarez (1983) formulation for atmospheric modeling and its numerous extensions in ocean modeling. In this paper, a novel feature of the new formulation is that it is based on integrating a Jacobian of ρ and the vertical coordinate z with respect to the vertical computational coordinate, i.e., it is based on the relation

$$\left(\frac{\partial p}{\partial x}\right)_z = \left(\frac{\partial p}{\partial x}\right)_{z=\zeta} + \frac{g}{\rho_0} \int_s^0 \left\{ \frac{\partial z}{\partial s'} \frac{\partial \rho}{\partial x} - \frac{\partial z}{\partial x} \frac{\partial \rho}{\partial s'} \right\} ds', \quad (1.2)$$

where x, s are the generalized topography-following coordinates and $z = \zeta$ is the position of the free surface. Note that the gradient is applied on the density before the integration is done. Equations (1.1) and (1.2) are analytically equivalent, but their discretized forms may differ. Based on the new formulation, we design numerical schemes which minimize truncation errors and retain some important integral properties of the continuous equations. Conservation of momentum, total energy and bottom pressure torque are considered in Part II.

The secondary goals of this study are to examine the performance of the proposed schemes in ocean modeling applications and to provide guidance for their use. In this paper, we examine the formulation of the pressure gradient force in two steps. First, we analytically examine the truncation error and consider the implications for hydrostatic inconsistency. Second, we examine the pressure gradient error in two sets of diagnostic calculations, the first with realistic vertical variations, but horizontally uniform density and the second with both vertical and horizontal variations in density. Results are compared with analytical solutions in order to evaluate the effectiveness of the vertical weighting scheme and the use of non-uniform vertical resolution. In a companion paper (Part II), we concentrate on discrete consistency and the performance of the new formulation in realistic, prognostic ocean modeling applications.

2 The Pressure Gradient Formulation

In this section, we derive the Jacobian form of the pressure gradient force in both analytical and discrete forms. Without loss of generality, we restrict attention to two dimensions, x and z .

2.1 Analytical formulation

Let x^*, z, t be the Cartesian coordinate system (or z -system) and let x, s, t be the generalized topography-following coordinate system (or s -system). A single-valued monotonic relationship between z and s is assumed such that

$$z = z(x, s, t) \quad -1 \leq s \leq 0 .$$

Some particular examples, including Phillips' (1957) σ -system, Song and Haidvogel's (1994) s -system and the isopycnal coordinate system, are given in Appendix A.

With the hydrostatic approximation, and using p to represent the pressure divided by the reference density, ρ_0 , the horizontal pressure gradient in the x^* -direction of the momentum equations is given by

$$\left. \frac{\partial p}{\partial x^*} \right)_z = \left. \frac{\partial p}{\partial x^*} \right)_{z=\zeta} - \int_z^\zeta \left. \frac{\partial b}{\partial x^*} \right)_{z'} dz' , \quad (2.1)$$

where $\zeta = \zeta(x, y, t)$ is the sea surface elevation and $b = -g\rho/\rho_0$ is the buoyancy. The $)_z$ -symbol emphasizes that the derivative is carried out with z held constant, otherwise with s held constant. Using the chain rule we have

$$\left. \frac{\partial b}{\partial x} = \frac{\partial b}{\partial x^*} \right)_z + \frac{\partial b}{\partial z} \frac{\partial z}{\partial x} ,$$

and factoring out $\partial z/\partial s$, then rearranging terms gives

$$\left. \frac{\partial b}{\partial x^*} \right)_z = \frac{\partial s}{\partial z} \left\{ \frac{\partial z}{\partial s} \frac{\partial b}{\partial x} - \frac{\partial z}{\partial x} \frac{\partial b}{\partial s} \right\} . \quad (2.2)$$

Substituting into equation (2.1) we obtain the Jacobian form of the pressure gradient:

$$\left. \frac{\partial p}{\partial x^*} \right)_z = \left. \frac{\partial p}{\partial x^*} \right)_{z=\zeta} - \int_s^0 \left\{ \frac{\partial z}{\partial s'} \frac{\partial b}{\partial x} - \frac{\partial z}{\partial x} \frac{\partial b}{\partial s'} \right\} ds' . \quad (2.3)$$

Clearly, vertical variations in the horizontal pressure gradient are simply given by an integral of the Jacobian,

$$J(z, b) = \frac{\partial z}{\partial s} \frac{\partial b}{\partial x} - \frac{\partial z}{\partial x} \frac{\partial b}{\partial s} . \quad (2.4)$$

It should be noted that the formulation in terms of a Jacobian is significant since it is clearly independent of the particular form of the vertical coordinate. As examples, in

Cartesian coordinates $s = z$ and $J(z, b) = \frac{\partial b}{\partial x} \Big|_s = \frac{\partial b}{\partial x^*} \Big|_z$; in σ -coordinates $s = \sigma = (z - \zeta)/H$ and $J(z, b) = H \frac{\partial b}{\partial x} - \frac{\partial b}{\partial \sigma} \frac{\partial \sigma}{\partial x}$, where $H = h + \zeta$; and in isopycnal coordinates $s = \rho$ and $J(z, b) = -\frac{g}{\rho_0} \frac{\partial z}{\partial x} \Big|_\rho$.

2.2 Discrete Formulation

The pressure gradient formulation discussed here can be used with essentially any numerical scheme. We have chosen to make use of an Arakawa C-grid (Arakawa and Lamb 1977) in the horizontal and a staggered grid (Grid 4 as in Leslie and Purser, 1992) in the vertical (Fig. 1). The staggered vertical grid, as reviewed by Leslie and Purser (1992), has the attractive feature that the variables u , v and ρ are staggered relative to p and ω (or \dot{s} , the vertical velocity in the s -coordinate) so that integral quadrature of the continuity and hydrostatic equations is easily implemented using the “natural” control volume approach.

To derive discrete schemes for the horizontal component of the pressure gradient, we will use the following differencing and averaging operators:

$$\begin{aligned}
 \delta_x b &= b_{i+1} - b_i \quad , \\
 \delta_s b &= b_{k+1} - b_k \quad , \\
 \bar{b}^x &= \frac{1}{2}(b_i + b_{i+1}) \quad , \\
 \bar{b}^s &= \frac{1}{2}(b_k + b_{k+1}) \quad , \\
 \tilde{b}^s &= \alpha b_k + \beta b_{k+1} \quad , \\
 \bar{b}_c &= \frac{1}{2}(\bar{b}_k^x + \bar{b}_{k+1}^x) \quad , \\
 \tilde{b}_c &= \alpha \bar{b}_k^x + \beta \bar{b}_{k+1}^x,
 \end{aligned} \tag{2.5}$$

where indices i and k represent discrete locations in the horizontal, x , and vertical, s , directions, respectively. The superscripts x and s indicate averaging in these directions, and the subscript c indicates averaging over the local stencil to give a mean value, as illustrated in Fig.1. An overbar always corresponds to a simple centered mean. The weighting factors, α and β are included to allow us to choose the vertical level at which the Jacobian is evaluated. A tilde is used to indicate an optimal choice for these coefficients (discussed below).

If the Jacobian is computed at the stencil center with respect to x and s , the pressure difference across the grid cell at the k th level can be obtained by integrating from the surface:

$$PX_k = PX_\zeta - \sum_{k'=k}^K \delta \mathcal{J}_{i+\frac{1}{2}, k'+\frac{1}{2}}, \quad (2.6)$$

where $\delta \mathcal{J}$ is the discrete form of $J(z, b) dx ds$, which will be discussed next. PX_ζ is the value of the pressure difference at the surface, and $k = 1$ and K correspond to the bottom and top levels, respectively. If a staggered vertical grid is used as shown in Fig.1, the top level $k = K$ is a half level and the Jacobian is computed similarly to the other levels (see below), but using appropriate surface boundary conditions to estimate derivatives at the upper level.

The Standard Jacobian

The simplest discrete analogue of the Jacobian is the second order central difference scheme,

$$\delta \mathcal{J} = \delta_s \bar{z}^x \delta_x \bar{b}^s - \delta_x \bar{z}^s \delta_s \bar{b}^x. \quad (2.7)$$

We refer to this scheme as the “standard Jacobian” since it uses standard centered differences in the s -coordinate system. It is noteworthy that this scheme corresponds to fitting the bilinear form

$$b = b_c + \left(\frac{\partial b}{\partial x} \right)_c (x - x_c) + \left(\frac{\partial b}{\partial s} \right)_c (s - s_c) + \left(\frac{\partial^2 b}{\partial x \partial s} \right)_c (x - x_c)(s - s_c) \quad (2.8)$$

over each grid cell of the model, resulting in a well defined, continuous approximation to the density field over the entire domain. In practise, the finite difference approximations for s and its derivatives are also consistent with s being consistently represented by a bilinear function of x and z over each grid cell (see (2.16)). Thus, if the density could actually be represented by a bilinear function of x and s over each grid cell, then each term in (2.7), and hence also the pressure gradient results, would be exact.

This scheme can be easily implemented in any numerical model with any desired stretching of the vertical coordinate. In the case of the z -system, the second term in (2.7) vanishes and it leads to the usual Cartesian formulation. In the case of σ -coordinates, it gives a scheme

equivalent to that discussed by Mellor et al. (1994) with a uniform σ grid. In the case of an isopycnal-system, the first term in (2.7) vanishes and it gives the pressure gradients on isopycnal surfaces.

A bilinear approximation in x and s is probably near optimal for fitting buoyancy variations associated with plumes on continental slopes, but this structure will not be optimal in all cases. Indeed, gravity and rotational effects combine to cause most features (in particular, those associated with eddies and large scale currents) in the ocean to have a small vertical to horizontal aspect ratio. Hence, even after removing the domain averaged vertical buoyancy profile most of the remaining buoyancy anomalies will be approximately aligned with the horizontal. To better deal with such buoyancy anomalies, we now consider an alternative formulation designed to give improved results when the buoyancy variations are well approximated by a bilinear function of x and z over each grid cell.

The Weighted Jacobian

In this subsection, we determine the optimal choice for the weighting factor α for the particular case when the buoyancy varies bilinearly with x and the depth coordinate, z . Before doing so we record the following relationships since they prove useful in the algebraic manipulations.

$$\begin{aligned}
\bar{b}_{i+1}^s - \bar{b}_c &= \frac{1}{2} \delta_x \bar{b}^s , \\
\bar{b}_i^s - \bar{b}_c &= -\frac{1}{2} \delta_x \bar{b}^s , \\
\bar{b}_{k+1}^x - \bar{b}_c &= \frac{1}{2} \delta_s \bar{b}^x , \\
\bar{b}_k^x - \bar{b}_c &= -\frac{1}{2} \delta_s \bar{b}^x , \\
\bar{b}_{k+1}^x - \tilde{b}_c &= \alpha \delta_s \bar{b}^x , \\
\bar{b}_k^x - \tilde{b}_c &= -\beta \delta_s \bar{b}^x .
\end{aligned} \tag{2.9}$$

In general, the vertically weighted Jacobian is given by:

$$\delta \tilde{\mathcal{J}} = \delta_s \bar{z}^x (\alpha \delta_x b_k + \beta \delta_x b_{k+1}) - (\alpha \delta_x z_k + \beta \delta_x z_{k+1}) \delta_s \bar{b}^x , \tag{2.10}$$

where α and $\beta (= 1 - \alpha)$ are the weighting factors. The standard scheme, centered in the stretched coordinate s , corresponds to $\alpha = \frac{1}{2}$. We now determine α such that exact pressure difference results are obtained for a buoyancy disturbance of the general form $b(x, z) = b_0(x) + b_1(x)z$. In this case, the exact pressure difference at depth z is given by:

$$PX_k = PX_\zeta - \sum_{k'=k}^K [\delta_x b_0 + \bar{z}_c \delta_x b_1] \delta_s \bar{z}^x, \quad (2.11)$$

where $\bar{z}_c = (z_1 + z_2 + z_3 + z_4)/4$, and the z_i are the z -levels of the corners of the control volume.

Note that the vertical variation in the pressure difference across a cell depends only on the densities along the side-walls of the column considered, and not on the interior values. Thus, pressure differences will depend on the differences in b_0 and b_1 across the cell and not on details of the horizontal buoyancy variations within the cell, exactly as for the usual Cartesian coordinate system.

First, consider $b = b_0(x)$. In this case, $\delta_s b_0(x) = 0$, and

$$\delta \tilde{\mathcal{J}} = \delta_s \bar{z}^x \delta_x b_0(x),$$

which gives the exact pressure difference as required in (2.11). Note that this places no restriction on the weighting factor α .

Now consider $b = b_1(x)z$. In this case,

$$\begin{aligned} \delta \tilde{\mathcal{J}} &= \delta_s \bar{z}^x \{ \alpha \delta_x [b_1(x)z]_k + \beta \delta_x [b_1(x)z]_{k+1} \} - \{ \alpha \delta_x z_k + \beta \delta_x z_{k+1} \} \delta_s [\overline{b_1(x)z}] \\ &= \delta_s \bar{z}^x \left\{ \alpha \left[\left(\bar{b}_{1c} + \frac{1}{2} \delta_x b_1 \right) z_{i+1,k} - \left(\bar{b}_{1c} - \frac{1}{2} \delta_x b_1 \right) z_{i,k} \right] \right. \\ &\quad \left. + \beta \left[\left(\bar{b}_{1c} + \frac{1}{2} \delta_x b_1 \right) z_{i+1,k+1} - \left(\bar{b}_{1c} - \frac{1}{2} \delta_x b_1 \right) z_{i,k+1} \right] \right\} \\ &\quad - \frac{1}{2} [\alpha (z_{i+1,k} - z_{i,k}) + \beta (z_{i+1,k+1} - z_{i,k+1})] \times \\ &\quad \left[\left(\bar{b}_{1c} + \frac{1}{2} \delta_x b_1 \right) \delta_s z_{i+1} + \left(\bar{b}_{1c} - \frac{1}{2} \delta_x b_1 \right) \delta_s z_i \right], \end{aligned}$$

which, after some straightforward algebra, may be rewritten as

$$\delta \tilde{\mathcal{J}} = \left[\delta_s \bar{z}^x \bar{z}_c - \frac{1}{4} \delta_x (\delta_s z) \delta_x \bar{z}^s \right] \delta_x b_1. \quad (2.12)$$

For consistency with (2.11), we require that

$$\left[\delta_s \bar{z}^x \tilde{z}_c - \frac{1}{4} \delta_x \delta_s z \delta_x \tilde{z}^s \right] \delta_x b_1 = \bar{z}_c \delta_s \bar{z}^x \delta_x b_1 \quad . \quad (2.13)$$

Clearly this condition places no restriction on the value of α if $\delta_x b_1 \equiv 0$. For a buoyancy field which varies linearly with z , but is independent of horizontal position, pressure gradients will be accurately represented for any weighting factor, including the uniform weighting, $\alpha = \beta = \frac{1}{2}$. Thus, there is no obvious advantage of any particular choice of weighting for the case of a horizontally uniform buoyancy field, which is often used as a test case.

Equation (2.13) shows that our weighting is determined to properly allow for horizontal changes in the vertical variations of the buoyancy field. Using this condition and the relations (2.5), some algebra gives

$$\begin{aligned} \alpha &= \frac{2(\delta_s \bar{z}^x)^2 - \delta_x(\delta_s z) \delta_x z_{k+1}}{4(\delta_s \bar{z}^x)^2 - (\delta_x \delta_s z)^2} \\ &= \frac{1}{2} - \gamma \quad , \end{aligned} \quad (2.14)$$

where

$$\gamma = \frac{\delta_x \bar{z}^s \delta_x(\delta_s z)}{4\delta_s z_{i+1} \delta_s z_i} \quad . \quad (2.15)$$

Clearly, our weighted Jacobian formulation corresponds to evaluation of the Jacobian at $x = x_c$ and $s = \alpha s_k + \beta s_{k+1} = (s_k + s_{k+1})/2 + \gamma(s_{k+1} - s_k)$.

Below, we show that this corresponds to the position $x = x_c, z = \bar{z}_c$ in the x, z coordinate system, i.e., the Jacobian is centered in the z -coordinate system. First, we express s in terms of the Cartesian coordinates x and z , as

$$s = s_c + \left(\frac{\partial s}{\partial x} \right)_c (x - x_c) + \left(\frac{\partial s}{\partial z} \right)_c (z - \bar{z}_c) + \left(\frac{\partial^2 s}{\partial x \partial z} \right)_c (x - x_c)(z - \bar{z}_c) \quad . \quad (2.16)$$

Note that the point (x_c, \bar{z}_c) in x, z -space is equivalent to the point (x_c, s_c) in x, s -space.

Defining s_i such that (x_i, s_i) corresponds to the point (x_i, z_i) , we have the relations

$$s_1 = s_c - \left(\frac{\partial s}{\partial x} \right)_c \frac{\delta x}{2} + \left(\frac{\partial s}{\partial z} \right)_c (z_1 - \bar{z}_c) - \left(\frac{\partial^2 s}{\partial x \partial z} \right)_c \frac{\delta x}{2} (z_1 - \bar{z}_c)$$

$$\begin{aligned}
s_2 &= s_c + \left(\frac{\partial s}{\partial x}\right)_c \frac{\delta x}{2} + \left(\frac{\partial s}{\partial z}\right)_c (z_2 - \bar{z}_c) + \left(\frac{\partial^2 s}{\partial x \partial z}\right)_c \frac{\delta x}{2} (z_2 - \bar{z}_c) \\
s_3 &= s_c - \left(\frac{\partial s}{\partial x}\right)_c \frac{\delta x}{2} + \left(\frac{\partial s}{\partial z}\right)_c (z_3 - \bar{z}_c) - \left(\frac{\partial^2 s}{\partial x \partial z}\right)_c \frac{\delta x}{2} (z_3 - \bar{z}_c) \\
s_4 &= s_c + \left(\frac{\partial s}{\partial x}\right)_c \frac{\delta x}{2} + \left(\frac{\partial s}{\partial z}\right)_c (z_4 - \bar{z}_c) + \left(\frac{\partial^2 s}{\partial x \partial z}\right)_c \frac{\delta x}{2} (z_4 - \bar{z}_c)
\end{aligned} \tag{2.17}$$

Averaging these equations gives

$$s_c = \bar{s} - \frac{\delta_x \bar{z}^s \delta x}{4} \left(\frac{\partial^2 s}{\partial x \partial z}\right)_c \tag{2.18}$$

where

$$\bar{s} = \frac{s_1 + s_2 + s_3 + s_4}{4} . \tag{2.19}$$

Now, from (2.15) we have

$$\begin{aligned}
\gamma &= \frac{\delta_x \bar{z}^s \delta_x (\delta_s z)}{4 \delta_s z_{i+1} \delta_s z_i} \\
&= \frac{\delta_x \bar{z}^s}{4 \delta s} \left(\frac{\delta s}{\delta_s z_i} - \frac{\delta s}{\delta_s z_{i+1}} \right) \\
&= -\frac{\delta_x \bar{z}^s \delta x}{4 \delta s} \left(\frac{\partial^2 s}{\partial x \partial z}\right)_c ,
\end{aligned} \tag{2.20}$$

so that (2.18) can be rewritten as

$$s_c = \bar{s} + \gamma \delta s . \tag{2.21}$$

That is, γ gives the fractional change in s required to shift from the mid-point in s -space to the mid-point in z -space. Since the weighted Jacobian corresponds to evaluation of the Jacobian at $s = s_c$ (i.e., $z = \bar{z}_c$), this scheme is effectively centered in z -space rather than in s -space, as for the standard Jacobian. This is clearly consistent with the fact that the scheme has been designed to give exact results when the buoyancy field varies linearly with z (rather than s) over each grid cell. This is the only difference between the standard and weighted Jacobian formulations.

Note that the choice of γ given by (2.15) is independent of the buoyancy field: if the rigid lid approximation is made, it only needs to be calculated at the beginning of the model run. Even with a free surface, the rigid lid approximation to α might be used in some applications

with little loss of accuracy. Also note that for any uniform grid of parallelograms (including rectangles), $\delta_x(\delta_s z) = 0$, so $\alpha = \frac{1}{2}$ in this case, and the “weighted Jacobian” reduces to the “standard Jacobian”, as expected. The two schemes differ only in the case of a non-uniform grid.

3 Analytical Error Analysis

Haney (1991) systematically analyzes the errors associated with computing the pressure gradient force over steep topography in σ -coordinate ocean models. His analysis is based on the fact that a pressure gradient scheme should not generate any force if the surface pressure is constant and isopycnals are horizontal, i.e., $b = b(z)$. In this case, any nonzero value computed by the scheme is due to truncation error. In practice, a reference state $\bar{b}(z)$ is often removed from the buoyancy field and only the perturbation $b' = b(x, y, z, t) - \bar{b}(z)$ is used in computing the pressure gradient. The perturbation field $b'(x, y, z, t)$ clearly does not satisfy the above condition of horizontal uniformity. Further, we have already pointed out that the weighting factor in the weighted Jacobian scheme is determined by horizontal variations in the vertical stratification, and this effect is clearly not addressed through the consideration of a horizontally uniform buoyancy field. Nevertheless, this special case is of interest since large scale buoyancy variations will generally result in there being vertical structure in the horizontal mean buoyancy perturbation over the local stencil. Further, results for this special case help to reveal potential problems with topography-following coordinate systems and particular advantages of different numerical schemes.

Haney discusses four aspects of the errors that occur in the conventional σ -coordinate formulation of (1.1):

- Errors associated with a buoyancy field which is independent of z . In this case, he shows that the numerical form commonly used is exact.
- Errors associated with isopycnal perturbations which are a linear function of z , i.e.,

$b' = b_0 + N_0^2 z$. For this case, he finds that the error is proportional to

$$\varepsilon_k = \left(\frac{\delta\sigma_k}{2} \right)^2 - \sum_{k'=1}^K \left(\frac{\delta\sigma_{k'}}{2} \right)^2 \delta\sigma_{k'} \quad .$$

This error is zero only for a uniform vertical grid.

- The (so-called) hydrostatic inconsistency error.
- Errors associated with the buoyancy profiles corresponding to the first three baroclinic Rossby modes.

The first two kinds of disturbance errors should vanish exactly in models of second order accuracy. Unfortunately, for the case of non-uniform vertical grid spacing the accuracy of the scheme will typically reduce to first order in the grid spacing (Chen and Beardsley, 1995). As noted by Haney (1991), if the sigma grid spacing is smaller near the surface and larger at depth, ε_k will be negative in the upper ocean and positive in the deep ocean. The resulting erroneous pressure gradient will tend to produce a geostrophic flow along the isobaths with shallow water to the right in the upper layers and to the left in the lower layers.

We know from the previous section (see (2.13) and the associated discussion) that the new formulations introduced here give exact representations of the pressure gradient force if the buoyancy is horizontally uniform and varies linearly with z in the vertical direction. In addition, by choosing s to be an appropriately stretched coordinate, surface and bottom layers can be well resolved without introducing non-uniform s -levels, so second order accuracy in the vertical grid spacing is retained. This is an important advantage of using the present formulation in combination with generalized s -coordinates. We next analytically consider truncation errors and hydrostatic inconsistency.

Truncation Errors and Hydrostatic Inconsistency

Researchers have known about the so-called hydrostatic inconsistency associated with the σ -coordinate system for a long time. In meteorology, Rouseau and Pham (1971), Janjic (1977), and Mesinger (1982) discuss problems associated with violation of the condition

$$\left| \frac{\sigma}{D} \frac{\partial D}{\partial x} \right| \delta x < \delta \sigma \quad . \quad (3.1)$$

If this inequality is not satisfied, then an error occurs in the estimation of the horizontal pressure gradient which does not tend to zero as the vertical resolution is increased, a problem which is commonly referred to as hydrostatic inconsistency. Haney (1991) investigates the problem of hydrostatic inconsistency in some detail within an oceanographic context.

Mellor, et al. (1994) emphasize that the pressure gradient error in their formulation is not numerically divergent: instead, it is proportional to the difference between two terms which decrease as the square of the vertical and horizontal grid element sizes, respectively. Their equation (7) clearly reveals the source of the error minimum as a function of vertical resolution, which Haney (1991) discusses. This minimum is the result of cancelation of truncation errors associated with finite vertical and horizontal resolutions: neither of these errors actually increases beyond the point where the minimum error occurs.

From the derivations given in the previous section, we know that the standard formulation gives exact results if the buoyancy varies bilinearly with x and s over each grid cell. If the buoyancy field actually varies linearly with x , but nonlinearly with s , then a bilinear function of x and s over each grid cell becomes a better approximation to the real buoyancy field as the vertical resolution is improved, and we expect this scheme to converge to the correct answer as the vertical resolution is improved. Thus, for these special buoyancy profiles, the standard Jacobian formulation has a clear advantage. On the other hand, if the real buoyancy field varies linearly with x and nonlinearly with z , then increasing the vertical resolution in the s -coordinate system will not necessarily give improved results using either the standard or weighted Jacobian formulations. This is simply a consequence of the fact that reducing the increment in s will not significantly reduce the range of z values within a cell if the cell is near the bottom over steep bottom topography.

To give quantitative results on hydrostatic inconsistency, we now derive the truncation errors associated with our two schemes for the special case of a buoyancy field which is a quadratic function of z alone. For the special case of horizontal isopycnals, any vertical variation in the pressure difference across a cell must be due to truncation error. Expanding

$b(z)$ around an arbitrary vertical level, z_c , gives

$$b(z) = b_c + \left(\frac{\partial b}{\partial z}\right)_c [z - z_c] + \left(\frac{\partial^2 b}{\partial^2 z}\right)_c \frac{[z - z_c]^2}{2} + \text{higher order terms} , \quad (3.2)$$

and inserting this expression into the Jacobian scheme, we obtain (after considerable algebra) the truncation error in the horizontal pressure difference change over the vertical extent of a single cell:

$$\text{Error} = \left\{ \frac{1}{4} \delta_x (\delta_s z) [(\delta_s \bar{z}^x)^2 - (\delta_x \bar{z}^s)^2] + \gamma \delta_x \bar{z}^s [\delta_s z_{i+1} \delta_s z_i] \right\} \left(\frac{\partial^2 b}{\partial^2 z}\right)_c + \text{higher order terms} . \quad (3.3)$$

For the standard Jacobian, $\gamma = 0$ and the second term vanishes. Neglecting the higher order terms, the truncation error becomes

$$E_{SJ} = \frac{1}{4} \delta_x (\delta_s z) [(\delta_s \bar{z}^x)^2 - (\delta_x \bar{z}^s)^2] \left(\frac{\partial^2 b}{\partial^2 z}\right)_c . \quad (3.4)$$

For our weighted Jacobian, γ is given by (2.14), and (3.3) reduces to

$$E_{WJ} = \frac{1}{4} \delta_x (\delta_s z) (\delta_s \bar{z}^x)^2 \left(\frac{\partial^2 b}{\partial^2 z}\right)_c . \quad (3.5)$$

As expected, in either case the truncation error vanishes if b is solely a linear function of z . The weighted Jacobian offers no obvious advantage in this case. However, if $b(z)$ varies nonlinearly over the depth of a cell, the two schemes have distinctly different properties.

For the standard Jacobian ($\gamma = 0$), (3.4) is the generalization to arbitrary vertical coordinate of equation (7) in Mellor et al. (1994). For the special case of σ -coordinates, $\delta_s \bar{z}^x = h \delta \sigma$ and $\delta_x \bar{z}^s = \sigma \delta x \partial h / \partial x$ and our formula gives their equation. It is also clear that the generalization of the hydrostatic consistency condition (3.1) is

$$|\delta_x \bar{z}^s| \leq \delta_s \bar{z}^x , \quad (3.6)$$

which is reputed to be required to obtain optimal accuracy with topography following coordinates. In fact, from (3.4), we see that optimal accuracy is actually achieved at the point of equality, i.e., when equality is satisfied in (3.6). This error minimum for the standard Jacobian formulation is easily explained. If the vertical resolution is further reduced without

reducing the horizontal resolution, then interpolation in x or extrapolation in z is required to estimate the horizontal buoyancy difference across the grid cell. However, values slightly exceeding the point of equality will not be much worse than slightly smaller values. This is true for any s -coordinate system, including σ -coordinates.

From (3.5) we see that, for the weighted Jacobian, the term with $(\delta_x \bar{z}^s)^2$ is canceled from the truncation error. Thus, for a buoyancy profile that is quadratic in the vertical, the error converges monotonically to zero as the number of vertical levels increases (i.e., with decreasing $\delta_s \bar{z}^x = \bar{h} \delta \sigma$ in the σ -system). Note that the error cancelation which the standard Jacobian benefits from does not benefit the weighted Jacobian because it requires the density difference at the mean z level rather than at the mean s level at which the buoyancy difference is known when the opposite corners of a cell are at the same z level.

To illustrate the effect on velocity of the differences between the standard and weighted Jacobian schemes, we consider a density perturbation field which varies quadratically in the vertical. Thus, we consider a density perturbation of the form

$$\rho(z) = \left(\frac{z + h_{max}}{h_{max}} \right)^2. \quad (3.7)$$

The bottom pressure gradient error obtained with the standard Jacobian using the uniformly spaced σ -system can be estimated by summing up (3.4) over the depth of the water column. The corresponding geostrophic current error, accumulated over the full depth of the water column, is given by:

$$V_\epsilon = \frac{g}{f\rho_0} \frac{8\epsilon}{100} \left\{ \frac{1}{K^2} - \left(\frac{\epsilon \delta x}{h} \right)^2 \left(\frac{1}{3} + \frac{1}{2K} + \frac{1}{6K^2} \right) \right\}, \quad (3.8)$$

where $\epsilon = \delta_x h / \delta x$ is the bottom slope and K is the number of vertical levels. It can be seen that the second term decreases with δx^2 , but does not converge to zero with increasing K . For the weighted Jacobian scheme, the term proportional to δx^2 is completely absent. Figure 2 shows the results for $h = 2000m$, $\epsilon = 0.05$ and horizontal resolutions of $\delta x = 10km$ and $\delta x = 20km$. The standard Jacobian scheme (solid lines) outperforms the weighted Jacobian scheme when the ‘‘hydrostatic consistency’’ condition is satisfied, but performs less well when

the condition is significantly violated. For large scale problems, the horizontal resolution is generally decreased for practical reasons and the condition for hydrostatic consistency may be strongly violated. In this case, the weighted Jacobian may give superior results to the standard Jacobian, with the gain in accuracy increasing as $(\delta_x h/h)^2$.

Comparison of Figs. 2a and 2b confirms that the error associated with the standard Jacobian scheme increases like $(\delta_x h/h)^2 \propto (\delta x)^2$ when the hydrostatic consistency condition is violated, while the error in the weighted Jacobian scheme (dashed lines) converges to zero with increasing K .

We emphasize that the standard Jacobian benefits from there being no need for vertical interpolation when the upper corner on one side of a cell is at the same z -level as the lower corner on the other side of the cell. The weighted Jacobian does not benefit from this cancellation because this configuration gives the density difference at the mid-level in s -space whereas the weighted Jacobian requires this difference at the mid-level in z -space. Thus, the standard Jacobian will be more accurate when equality is approximately satisfied in (3.6). This might, for example, be used to advantage in numerical studies of plumes over steep bottom topography. However, models often strongly violate this condition. As pointed out by Mellor et al. (1994), with 20 evenly spaced σ -levels in the vertical, this condition requires $\delta_x h/h < 0.05$ which is a very severe constraint in regions of steep topography. The weighted Jacobian is interesting with regard to this point since, for a horizontally uniform buoyancy field with quadratic dependence on z , the hydrostatic consistency problem is eliminated. That is, when the buoyancy field is horizontally uniform and varies as a quadratic function of z over the full vertical extent of each grid cell, the model accuracy can be improved by simply increasing the vertical resolution without concern about hydrostatic inconsistency.

4 Diagnostic Examples

To quantitatively examine truncation errors and hydrostatic inconsistency, we consider some specific diagnostic examples. In these examples, we first follow Haney and examine buoyancy variations which would be associated with the first three vertical Rossby wave modes. We then consider a diagnostic example which considers the errors associated with perturbations which include both horizontal and vertical variations in the buoyancy field.

4.1 Modal buoyancy profiles

To examine the error associated with realistic vertical variations in the buoyancy field, we consider the local buoyancy perturbations due to the first three Rossby wave modes in the presence of a prescribed mean buoyancy frequency. Note that these results simply consider the effect of different vertical variations in the buoyancy field: isopycnals are still horizontal so the analytical solution has no flow.

The vertical modes are first determined by solving the eigenvalue problem:

$$\frac{qf}{N(z)} \frac{d}{dz} \left(\frac{qf}{N(z)} \frac{dT_m}{dz} \right) = -\lambda_m T_m \quad , \quad (4.1)$$

with boundary conditions

$$T'(0) = T'(-\infty) = 0 \quad . \quad (4.2)$$

The analytical solution is known for $N(z) = 0.01 \times e^{z/h_s} \text{ s}^{-1}$, where, h_s is a reference depth and q is a dimensionless constant. The eigenfunctions and eigenvalues are

$$T_m = (-1)^m \cos(m\pi e^{z/h_s}) \quad (^\circ K) \quad (4.3)$$

and

$$\lambda_m = \left(\frac{m\pi q}{h_s} \right)^2 \quad . \quad (4.4)$$

We consider results corresponding to $h_s = 400 \text{ m}$, $h = 2000 \text{ m}$ and $q = 100$. The buoyancy frequency and the first three modes are plotted in Fig. 3 and are similar to the baroclinic Rossby modes calculated by Rienecker et al. (1987) for the west coast of North America,

except for the surface mixed layers. These modes have been used by Rienecker et al. to decompose and analyze dynamic variables. For example, the pressure can be expanded as

$$p = \sum_{m=0}^{\infty} p_m(x, y, t) T_m(z) .$$

The barotropic mode, $p_0 T_0$, accounts for about 91% of the variance in the pressure field for the region off Oregon, and the first three baroclinic modes account for about 7%, 1.2%, and 0.5%, respectively. These modes are thus relevant to the vertical structure of oceanic flows and will be used to investigate the pressure gradient errors. It should be pointed out that the profiles used here are slightly different from those used by Haney (1991), but there is no significant difference in numerical errors if Haney's profiles are used. We use the present profiles because the existence of analytical solutions offers some obvious convenience.

Let $b_m(z) = \alpha g T_m(z)$ represent the buoyancy disturbances, where $\alpha = 2.5 \times 10^{-4} \text{ K}^{-1}$ is the thermal expansion coefficient and g is the acceleration due to gravity. To compute the discrete pressure gradient force, we use a typical continental slope of 0.05 over an average depth of 2000 m. Since the actual pressure gradient force is known to be zero in this case, any nonzero value computed by the difference scheme is due to truncation error. The false pressure gradient can be expressed as an erroneous geostrophic current parallel to the isobaths, $V_\epsilon = P X_k / f \delta x$, where $f = 10^{-4} \text{ s}^{-1}$ is the Coriolis parameter.

Case A: No Hydrostatic Inconsistency ($\delta x = 1 \text{ km}$)

We first consider results obtained with $\delta x = 1 \text{ km}$ so that potential problems associated with hydrostatic inconsistency are avoided. The errors corresponding to the first three Rossby modes are shown in Fig. 4 for three different vertical resolutions: $K = 10, 20,$ and 30 . In each case, results are shown for the standard Jacobian scheme with uniformly spaced σ -coordinate (solid lines) and with the s -coordinate system introduced by Song and Haidvogel (1994), with $\theta = 3$ to improve the resolution in the region of strong vertical stratification (dashed lines). The results corresponding to the uniformly spaced σ -coordinate system were obtained by taking $\theta = 0$ in the latter s -coordinate system. The errors obtained with $\theta = 0$ using the new pressure gradient formulation are about half those computed by Haney based on the

standard formulation. This improvement is significant, but not particularly dramatic. Use of the weighted Jacobian scheme (results not shown) does not significantly reduce the errors for these calculations. This is not unexpected since our analytical results have suggested that the weighted Jacobian gives improved performance when there are horizontal variations in the vertical stratification in combination with a non-uniform vertical grid or when there are problems with hydrostatic consistency, neither of which are present in this example.

As noted above, a major advantage of using generalized s -coordinates is that non-uniform vertical grids can be used without giving up the second order accuracy of the numerical scheme. The particular s -coordinate system discussed by Song and Haidvogel (1994) provides an example of how this may be used to advantage. This coordinate system includes three parameters, h_c , b and θ , which can be used to adjust the vertical variations in the vertical resolution. $\theta = 0$ corresponds to the uniformly spaced σ -coordinate system and larger values of θ correspond to larger variations in the vertical resolution over the depth of the water column. h_c and b have no effect when $\theta = 0$, but for nonzero θ , h_c determines a vertical position above which the vertical resolution is nearly constant and maximized, and the value of b determines where increased resolution should be concentrated. h_c is always less than or equal to the minimum water depth within the region being modeled. Choosing $b = 0$ maximizes the resolution in the upper portion of the water column and $b = 1$ gives similar resolution near the surface and bottom. At the surface, the s -coordinate system nearly coincides with the z -coordinate system ($s = 0$ corresponds to the position of the free surface), so problems with the pressure gradient error are reduced in this region.

Since we know that our discretization scheme is well suited to the case where the buoyancy varies linearly over each individual grid cell, it is likely that results can be improved by choosing h_c , b and θ such that $N(z)$ is roughly constant over each grid cell. We thus set $b = 0$ and $h_c = 400$ m to force any increase in resolution to be concentrated in the near surface region where $N(z)$ varies most rapidly. We then experiment to determine that $\theta = 3$ gives a reasonable representation of $N(z)$ over the entire water column. With this choice of parameters, we find that with the standard Jacobian formulation the error is about a factor

of 10 smaller than that in the σ -coordinate system for each mode and for each choice of K (dashed lines in Fig. 4). Results are not significantly different for the weighted Jacobian formulation.

Clearly, an objective procedure could be developed to determine optimal parameter values in any s -coordinate system based on satisfying specific resolution criterion. The present example suggests that this may be worthwhile, but it has not yet been investigated. The main point of the present exercise is that errors can be dramatically reduced through an appropriate choice of the coordinate system, and by using an appropriately stretched grid, there need not be any reduction in the order of accuracy.

Case B: With Hydrostatic Inconsistency ($\delta x = 10$ km)

Next we consider examples which are intended to confirm our analytical predictions regarding hydrostatic inconsistency and to further examine its qualitative effects. We again follow Haney (1991) and consider a specific example in which the horizontal and vertical resolutions violate the condition (3.1) or (3.6). In particular, we consider horizontal grids with $\delta x = 10$ km, as opposed to the 1 km grid used above. With this value of δx , the consistency condition is violated for $K \geq 12$ with uniformly spaced σ -levels.

The largest truncation errors in the water column are shown in Fig. 5 as a function of K for the three different Rossby wave modes, using three different schemes: (a) the standard Jacobian in the σ -system; (b) the standard Jacobian in the s -system of Song and Haidvogel (1994) with $h_c = 1000m$ and optimal $\theta(K)$ by taking advantage of the error cancelation discussed in the previous section (see below); (c) the weighted Jacobian in the s -system with $\theta = 3$. In each case, the errors increase with mode number as expected. The errors in Fig. 5(a) corresponding to the standard Jacobian in the σ -system are similar to those presented in Fig. 7 of Haney (1991). Consistent with Haney's results, the error increases for $K \geq 10$. These results are similar to the results shown in Fig. 2 for a quadratic vertical profile and further confirm that the error minimum which has been associated with the hydrostatic consistency boundary is actually due to cancelation of the truncation errors due to finite horizontal and

vertical resolutions.

Results obtained with the standard Jacobian scheme in the s -system with optimal θ (Fig. 5(b)) show that errors are reduced substantially for this typical choice based on accurately representing the vertical stratification. In the present case, the improved representation of vertical stratification is accompanied by reduced hydrostatic inconsistency at depth due to coarser resolution there. Fig. 5(b) shows that, at least in some cases, problems with hydrostatic inconsistency can be substantially reduced with the standard Jacobian scheme if the vertical coordinate system is carefully chosen. In this case, the error continues to decrease with increasing K because the value of θ has been chosen such that the largest truncation errors associated with finite horizontal and vertical resolution cancel. That is, we have chosen θ such that equality in (3.6) is satisfied at the bottom. For $b = 0$ in the s -coordinate system of Song and Haidvogel (1994) (see Appendix A), this gives:

$$\theta = \frac{h_x \delta x}{h - h_c} K - \frac{h_c}{h - h_c}. \quad (4.5)$$

In Fig. 5(b), we have used $h_x = 0.05$, $\delta x = 10km$, $h = 2000m$, and $h_c = 1000$ m, which gives $\theta = 0.5K - 1$, and we see that this choice does indeed substantially reduce the model error.

However, from Fig. 5(c) we see that the minimum error as a function of K is not present, as expected from our analytical considerations. Comparing Fig. 5(b) and 5(c), reveals that the errors are actually increased in the weighted Jacobian scheme. This is a consequence of the error cancelation which the standard Jacobian formulation benefits from, but the weighted Jacobian formulation does not. We also note, in contrast to the results of Fig. 2, that the errors in the weighted Jacobian formulation do not continue to decrease as K is increased. This is a reflection of the fact that hydrostatic inconsistency is only eliminated for buoyancy profiles which vary quadratically with z over the full depth range of each grid cell. Clearly, these baroclinic modal buoyancy profiles do not satisfy this condition.

The results shown in Fig. 5 seem to suggest that the standard Jacobian formulation has a clear advantage over the weighted Jacobian formulation. This suggestion is somewhat misleading. As we noted following (2.13) the weighting used in the weighted Jacobian formulation

is determined by the combined effect of horizontal and vertical variations in the buoyancy field. Since the above example does not include horizontal variations in the buoyancy field, the possible advantage of the weighted Jacobian formulation is not considered by these tests. We now consider an example which includes both horizontal and vertical buoyancy variations in order to test the formulations under somewhat more realistic conditions.

4.2 Coastal Front

In the above two subsections, we have examined truncation errors due to isopycnal disturbances which are horizontally uniform, i.e., b is a function of z , only. In reality, ocean flows can be strongly stratified in both horizontal and vertical directions. Such cases are often seen in coastal oceans where the combination of complex coastal geometry and steep topography offer great challenges for numerical modelers.

Here, we consider a case with both vertical and horizontal variations in density, similar to the shelf-break front in the Middle Atlantic Bight (MAB). During the winter, the water column over the shelf and the upper slope is nearly linearly stratified in both temperature and salinity. However, a persistent, sharp shelf-break front is found near the shelf edge where the fresher, colder shelf water meets the saltier, warmer slope water. The accurate computation of the pressure gradient force over such a region of steep topography is potentially important for the study of frontal dynamics in the coastal ocean. Following Chapman and Gawarkiewicz (1993), the density field is approximated by:

$$\rho(x, z) = 24 + \{2.312 - 0.175(T - 10.5) + 0.779(S - 34)\} \times Z(z) \quad (4.6)$$

where

$$Z(z) = \left\{ 1 - \varepsilon \frac{z}{h_s} \right\},$$

and the surface temperature and salinity are given by

$$T = 10.5 + 2.5 \tanh[(x - L)/20] \quad (^\circ C)$$

$$S = 34 + \tanh[(x - L)/20] \quad (psu).$$

The corresponding density field is plotted in Fig. 6a, superimposed on the model topography from Gawarkiewicz and Chapman (1992). The topography includes a gently sloping continental shelf from 50 m depth at the coast to about 180 m depth at the shelfbreak, an adjacent steeply sloping region extending offshore to about 2000 m depth with a slope of 3%, and an abyssal plain. The widths of the shelf, slope and abyssal plain are 50 km, 50 km, and 100 km, respectively. The distance of the front from the coast is $L = 50$ km, the depth parameter $h_s = 150$ m, and $\varepsilon = 0.01$ determines the vertical gradient in the density field. Even in this case, where horizontal gradients are strong, removing the reference state is still worthwhile and this has been done in the examples presented below.

The exact pressure gradient force can be calculated analytically and the geostrophic estimate of the associated current, relative to the surface, is plotted in Fig. 6b. While this example does not consider the dynamics which determine the surface pressure field, it is well-suited to revealing problems with the representation of the pressure gradient force associated with the combination of horizontal and vertical variations in the buoyancy field. The errors in the geostrophic current estimated with the standard Jacobian and $\theta = 3$ are plotted in Fig. 6c and the corresponding errors obtained with the same value of θ , but using the weighted Jacobian scheme are plotted in Fig. 6d. The error is small in Fig. 6c ($\lesssim 0.00024ms^{-1}$), but the weighted Jacobian scheme (Fig. 6d) gives the exact pressure gradient force even over this steep topography. This is as expected since our vertical weighting factor was chosen to give zero error for a density field which varies linearly with z .

Of course, we expect some error to be introduced in the weighted Jacobian scheme if the vertical variation in density is not linear. To investigate the errors associated with horizontal variations in combination with nonlinear vertical density profiles, we now consider results for a density profile which varies exponentially with z . In particular, we consider a density field of the form (4.6), but with

$$Z(z) = \exp\left(-\varepsilon \frac{z}{h_s}\right) , \quad (4.7)$$

where $\varepsilon = 0.04$. Results corresponding to this density profile, with all other parameters exactly as in Fig. 6 are shown in Fig. 7. Maximum errors are increased substantially to

$0.001ms^{-1}$ and $0.00009ms^{-1}$ for the standard and weighted Jacobian schemes, respectively. However, each of these errors remains small in comparison with the maximum current speed which is approximately $0.55ms^{-1}$ (Fig. 7b). The effect of increasing the horizontal grid size from 5km to 20km is shown in Fig. 8. For each formulation, the maximum errors are increased by about a factor of 10, comparable with the expected factor of 16 based on the scheme being second order accurate in the grid resolution. Even at this coarse resolution, the errors would be tolerable for most applications: the maximum error is about 2.6% of the maximum current for the standard Jacobian and about 0.1% for the weighted Jacobian.

5 Summary and Conclusions

The pressure gradient formulation remains one of the most important issues in the design of numerical models with topography-following coordinate systems. In this paper, we have introduced a generalized method to compute the pressure gradient force based on integrating the Jacobian of density and vertical coordinate. The Jacobian formulation allows us to design a scheme which can be used with any vertical coordinate system. Two different schemes are considered in some detail: the standard Jacobian scheme which is exact for any topography provided the buoyancy field varies bilinearly with x and s over each grid cell; and the weighted Jacobian scheme which is exact for any topography provided the buoyancy field varies bilinearly with x and z over each grid cell. Both schemes retain second order accuracy in the presence of horizontal and vertical variations in both the density field and the vertical grid spacing.

For each of the schemes discussed here, finite differences are applied to the density field to estimate horizontal density gradients prior to integrating to determine the horizontal pressure gradients. Since the density is always approximated by a linear function of s , the pressure field is consistently approximated by a quadratic in the vertical coordinate over each grid cell. This contrasts with the conventional approach in which the density field is first integrated to determine the pressure which is then finite differenced to estimate horizontal pressure

gradients. In this case, the pressure is effectively quadratic in the vertical coordinate over each grid cell since it is obtained by integrating a linear function of density, but subsequent finite differences of the pressure field may not properly account for this quadratic dependence. By differentiating the density prior to integrating, the present numerical schemes avoid this inconsistency in a natural way.

The truncation error is examined analytically for horizontally uniform isopycnal disturbances, and quantitatively for particular horizontally and vertically varying isopycnal disturbances. The accuracy of the Jacobian schemes are improved significantly over conventional formulations based on finite differencing the pressure field. Consistent with the results of Mellor et al. (1994), we find that, for a horizontally uniform buoyancy field which varies quadratically in the vertical, the standard Jacobian scheme converges to the exact solution with the square of the horizontal and vertical grid sizes. In this case, we find that the weighted Jacobian converges quadratically with the vertical grid size, independent of the horizontal grid spacing. However, it should be emphasized that the latter result holds only for a buoyancy field which is horizontally uniform and varies quadratically with z over the full vertical extent of each grid cell.

A generalized hydrostatic consistency condition is derived which applies for an arbitrary s -coordinate system when the standard Jacobian formulation is used. Unfortunately, violation of the hydrostatic consistency condition may occur in some cases, particularly, in large-scale modeling problems. If the resolution can be chosen such that the hydrostatic consistency condition is not violated, then the errors associated with the standard Jacobian scheme can be reduced by choosing the coordinate system such that errors due to finite horizontal and vertical resolutions cancel. This corresponds to the situation in which the vertical integral error terms in (3.3) vanishes.

The weighted Jacobian scheme was developed in order to improve the accuracy of pressure gradients when density variations are better approximated by a bilinear function of x and z than by a similar function of x and s . We expect that this will often be the case, even

after the horizontally averaged density field has been removed, since the vertical to horizontal aspect ratio is small for many oceanic phenomena. Consideration of the truncation error for this scheme has shown that the optimal choice of the weighting parameter to account for horizontal variations in the stratification also removes the problem of hydrostatic inconsistency for horizontally uniform buoyancy fields that vary quadratically with z over the vertical extent of each grid cell. For such buoyancy profiles, the error associated with the weighted Jacobian scheme continues to decrease like $1/K^2$, where K is the number of grid cells in the vertical, even when the standard scheme would be hydrostatically inconsistent.

Unfortunately, tests with horizontally uniform buoyancy profiles reveal that the error associated with the weighted Jacobian scheme does not continue to decrease with K if the buoyancy is not a quadratic functions of z . Indeed, the cancelation of errors in the standard Jacobian gives it an advantage over the weighted Jacobian when the buoyancy field is horizontally uniform. However, the derivation of the weighting factor used in the weighted Jacobian formulation makes it clear that the advantage of this scheme should become evident when both horizontal and vertical buoyancy variations are present. Examination of the results corresponding to a front over strongly sloping bottom topography shows that this is indeed the case. It is apparent that each scheme has advantages under certain circumstances.

The schemes discussed here can be used to avoid pressure gradient errors associated with topography-following coordinates if the buoyancy field varies linearly in either s or z . For nonlinear vertical density profiles, care is still required to minimize truncation errors. Removal of the vertical stratification as much as possible is an important method of controlling this error. Further improvements can be achieved through the use of a stretched vertical grid that increases resolution in the vicinity of rapid vertical variations in the deviations from this mean profile. Second order accuracy in the grid spacing can be retained with a non-uniform vertical grid by using a generalized s -coordinate system such as that considered by Song and Haidvogel (1994). Examples based on Song and Haidvogel's coordinate system show that, in realistic situations, the accuracy can sometimes be improved by a factor of 10 or more through the choice of the coordinate system, without increasing the computational burden.

In practice, although the square of the grid size will not approach zero, the accumulation of error can be controlled if integral properties of the continuous system are retained. In Part II of this work, we show that integrated momentum, energy and bottom torque effects are accurately represented by the present schemes. This is proven theoretically and verified experimentally through examination of the results of prognostic integrations.

Acknowledgment: The new scheme proposed in this work was implemented in the S-Coordinate Rutgers University ocean Model (SCRUM) and fully tested at Rutgers University. The author is particularly grateful to Professor Dale Haidvogel for his support and guidance during this period. The author also wishes to thank Drs. Daniel Wright, Charles Hannah, and Z. Xu for their careful reading the manuscript and providing comments.

APPENDIX A:

Various Vertical Coordinates

z -coordinate system: The z -coordinate system is the most commonly used Cartesian coordinate system with the z -axis pointing vertically upwards and the xy -plane occupying the undisturbed water surface. In numerical ocean modeling, the grid size in the vertical direction can be easily arranged to allow the highest resolution near the surface and somewhat less resolution below the thermocline. However, difficulty is encountered in representing varying topography, especially near coastal boundaries where the ocean depth varies rapidly from shallow to deep water. In such cases, a z -coordinate will approximate the bottom as a series of steps. This may lead to difficulty in accurately representing the effects of steep bottom slopes.

σ -coordinate system (Phillip 1957): This coordinate transforms the irregular physical domain, bounded by free surface and varying bottom, to a fixed regular computational domain. The coordinate transformation can be written as

$$\sigma = \frac{z - \zeta}{H}, \quad -h \leq z \leq \zeta,$$

where $H = h(x, y) + \zeta(x, y, t)$. The advantage of this coordinate is that it accurately represents both the depth and the bottom slope. A disadvantage is that it cannot maintain equally high resolution near the surface layer independent of local depth. For example, if a coastal region with a minimum inshore depth of 50 m and a maximum offshore depth of 5000 m is represented by a σ -coordinate with 20 evenly spaced levels, the layer thicknesses are 2.5 m in the near-shore region and 250 m in the offshore region. This kind of resolution is not likely to represent surface mixing processes at all well in the deep ocean.

Hybrid coordinate system (Spall and Robinson 1990): The hybrid coordinate system is a combination of the z -coordinate for the upper part of the ocean, and the σ -coordinate

for the lower part of the ocean. The coordinate transformation can be written as

$$\sigma = \begin{cases} \frac{z}{z_c}, & -z_c \leq z \leq 0 \\ \frac{z-h+2z_c}{h-z_c}, & -h \leq z \leq -z_c. \end{cases}$$

However, the derivative of this coordinate is discontinuous across the interface z_c , and a matching condition must be applied at this location.

s-coordinate system (Song and Haidvogel 1994): The s -coordinate system is designed to permit uniformly high resolution near the surface like the z -coordinate and preserve the bottom following character of the σ -coordinate. Its formulation consists of three terms:

$$z = \zeta(1 + s) + h_c s + (h - h_c)C(s), \quad -1 \leq s \leq 0,$$

where $C(s)$ is a set of s -curves, defined by

$$C(s) = (1 - b) \frac{\sinh(\theta s)}{\sinh \theta} + b \frac{\tanh[\theta(s + \frac{1}{2})] - \tanh(\frac{1}{2}\theta)}{2 \tanh(\frac{1}{2}\theta)},$$

where θ and b are the surface and bottom control parameters. Typical parameter ranges are $0 \leq \theta \leq 20$ and $0 \leq b \leq 1$, respectively. h_c is a constant chosen to be the minimum depth of the bathymetry or a width of surface or bottom boundary layer in which a higher resolution is required. Features of this s -coordinate system include that the σ -coordinate system is recovered as a special case by setting $\theta = 0$, it has a simple linear functional dependence on $\zeta(x, y, t)$ and $h(x, y)$, and z is a continuously differentiable function of s . With an equal grid step in s , and by choosing the parameter θ appropriately, the highest resolution is achieved near the surface layer ($b = 0$) or near surface and bottom ($b = 1$), independent of the varying bottom topography.

Isopycnal coordinate system: Different from all of the above vertical coordinates which are either fixed or nearly fixed in space, the isopycnal coordinate system is determined such that computational levels follow density surfaces, $\rho = \rho(x, y, z, t)$. This system is more natural for the large-scale ocean circulation because thermocline trajectories are believed to be largely tangential to density surfaces. However, it suffers from the same problems with the resolution of steep topography as the z -coordinate models do since isopycnals do not generally conform to the topographic variations.

References

- [1] Arakawa, A., and V. R. Lamb, 1977: Computational design of the basic dynamic processes of UCLA general circulation model, in *Methods in Comput. Phys.*, (Academic Press, New York/London, 1977), **17**, 173.
- [2] Arakawa, A. and M. J. Suarez, 1983: Vertical differencing of the primitive equations in Sigma Coordinates, *Mon. Wea. Rev.*, **111**, 34-45.
- [3] Arakawa, A. and C. S. Konor, 1996: Vertical differencing of the primitive equations on the Charney-Phillips grid in hybrid $\sigma - p$ vertical Coordinates, *Mon. Wea. Rev.*, **124**, 511-528.
- [4] Batteen, M. L., 1988: On the use of sigma coordinates in large-scale ocean circulation models, *Ocean Modeling*, **77**, 3-5.
- [5] Beckmann, A., and D.B. Haidvogel, 1993: Numerical simulation of flow around an isolated seamount, Part I: problem formulation and model accuracy, *J. Phys. Oceanogr.*, **23**, 1736-1753.
- [6] Bleck, R., 1978: Finite difference equations in generalized vertical coordinates. Part I: total energy conservation, *Contrib. Atmos. Phys.*, **51**, 360-372.
- [7] Blumberg, A. F., and G. L. Mellor, 1987: A description of a three-dimensional coastal ocean circulation model. Vol. 4, *Three-Dimensional Coastal Ocean Models*. N. Heaps, Ed., AGU, 208 pp.
- [8] Chapman, D. C., and G. Gawarkiewicz, 1993: On the establishment of the seasonal pycnocline in the Middle Atlantic Bight, *J. Phys. Oceanogr.*, **23**, 2487-2492.
- [9] Chen, C., and R. C. Beardsley, 1995: A numerical study of stratified tidal rectification over finite-amplitude banks. Part I: Symmetric banks, *J. Phys. Oceanogr.*, **25**, 2090-2110.

- [10] Fortunato, A.B. and A.M. Baptista, 1996: Evaluation of horizontal gradients in sigma-coordinate shallow water models, *Atmosphere-Ocean*, **34**, 489-514.
- [11] Gawarkiewicz, G. and D. C. Chapman, 1992: The role of stratification in the formation and maintenance of shelf- break fronts. *J. Phys. Oceanogr.*, **22**, 753-772.
- [12] Gerdes, R., 1993: A primitive equation ocean circulation model using a general vertical coordinate transformation, I. Description and testing of the model, *J. Geophys. Res.*, **98** (C8), 14,683-14,701.
- [13] Glenn, S., M. Crowley, D. Haidvogel and Y. Song, 1996: Underwater observatory captures coastal upwelling events off New Jersey, *EOS, Transactions, AGU*, **77** (25), 233, 236.
- [14] Haney, R. L., 1991: On the pressure gradient force over steep topography in sigma coordinate ocean models, *J. Phys. Oceanogr.*, **21**, 610-619(1976).
- [15] Janjic, Z. I., 1977: Pressure gradient force and advection scheme used for forecasting with steep and small scale topography, *Contrib. Atmos. Phys.*, **50**, 186-199.
- [16] Leslie, L. M., and R. J. Purser, 1992: A comparative study of the performance of various vertical discretization schemes, *Meteorol. Atmos. Phys.*, **50**, 61-73.
- [17] Mahrer, Y., 1984: An improved numerical approximation of the horizontal gradients in a terrain-following coordinate system, *Mon. Weat. Rev.*, **112**, 918-922.
- [18] Mellor, G.L., and T. Ezer, 1991: A Gulf Stream model and an altimetry assimilation scheme. *J. Geophys. Res.*, **96**, 8779-8797.
- [19] Mellor, G.L., T. Ezer, and L.-Y. Oey, 1994: The pressure gradient Conundrum of sigma coordinate ocean models, *J. Atmos. Ocean Tech.*, **11**(4), 1126-1134.
- [20] Mesinger, F., 1982: On the convergence and error problems of the calculation of the pressure gradient force in sigma coordinate models, *Geophys. Astrophys. Fluid Dyn.*, **19**, 105-117.

- [21] Oey, L-Y., G. L. Mellor, and R. I. Hires, 1985: A three-dimensional simulation of the Hudson-Raritan estuary. Part I: Description of the model and model simulations, *J. Phys. Oceanogr.*, **15**, 1676-1692.
- [22] Phillips, N. A., 1957: A coordinate system having some spatial advantages for numerical forecasting, *J. Meteorol.*, **14**, 184-186.
- [23] Rienecker, M. M., C. N. K. Mooers and A. R. Robinson, 1987: Dynamical interpolation and forecasts of the evolution of mesoscale features off Northern California, *J. Phys. Oceanogr.*, **17**, 1189-1213.
- [24] Rousseau, D., and H. L. Pham, 1971: Premiers resultat D'un modele de prevision numerique a courte echeance sur l'Europe. *La Meteorologie*, **20**, 1-12.
- [25] Smagorinsky, J., Strickler, R. F., Sangster, W. E., Manabe, S., Holloway, J. L. Jr., and Hembree, G. D., 1967: Prediction experiments with a general circulation model, *Proc. Intern. Symp. on Dynamics of Large Scale Atmospheric Processes*, Moscow, 23-30 June 1965, 70-134.
- [26] Spall, M. A., and A. R. Robinson, 1990: Regional primitive equation studies of the Gulf Stream meander and ring formation region, *J. Phys. Oceanogr.*, **20**, 985-1016.
- [27] Song, Y. and D. Haidvogel, 1993: Numerical simulations of the CCS under the joint effects of coastal geometry and surface forcing, in *Estuarine and Coastal Modeling* edited by M. L. Spaulding et al., 216-234.
- [28] Song, Y. and D. Haidvogel, 1994: A semi-implicit ocean circulation model using a generalized topography-following coordinate system, *J. Comput. Physics*, **115** (1), 228-244.
- [29] Sundqvist, H., 1975: On truncation errors in sigma-system models, *Atmosphere*, **13**, 81-95.
- [30] Zebiak, S. E., and M. A. Cane, 1987: A model El Nino-Southern Oscillation, *Mon. Weat. Rev.*, **115**, 2262-2278.

- [31] Zhu, Z., J. Thuburn, B. J. Hoskins, and P. H. Haynes, 1992: A vertical finite-difference scheme based on a hybrid $\sigma - \theta - p$ coordinate, *Mon. Weat. Rev.*, **120**, 851-862.

Figure Captions

Figure 1: The computational stencil of the Arakawa C-grid in the horizontal, and a staggered grid in the vertical. The open circles are the locations of ρ and s , and the squares are the locations of u . The solid dot indicates the evaluation position for $\delta J_{i+\frac{1}{2}, k+\frac{1}{2}}$.

Figure 2: Theoretical estimates of the bottom level geostrophic currents caused by the pressure gradient force error as a function of the number of vertical levels (K) for a density profile which varies quadratically in the vertical. The solid lines show results predicted for the standard Jacobian and the broken lines show the results for the weighted Jacobian.

Figure 3: The vertical profiles of the buoyancy frequency ($\text{cph} \times 1000$) and the first three baroclinic Rossby modes (1°K) computed for a 2000 m deep ocean with stratification representative of the California Current region.

Figure 4: Vertical profiles of the pressure gradient force error using three different vertical resolutions ($K=10, 20, 30$) disturbed by the first three baroclinic Rossby modes. Solid lines indicate results computed with a uniformly spaced σ -system and dash lines correspond to results obtained with Song and Haidvogel's s -system with $\theta = 3$.

Figure 5: Maximum value of the pressure gradient error as a function of the number of vertical levels (K) for vertical density profiles corresponding to the first three Rossby wave modes. Results for the three modes are shown in each frame. The larger errors correspond to the higher modes which generally contain less of the variance under realistic conditions. The three frames show results corresponding to three different approaches: (a) the standard Jacobian scheme in σ -system; (b) the standard Jacobian scheme in the s -system with θ chosen to minimize truncation errors; (c) the weighted Jacobian scheme in the s -system with $\theta = 3$.

Figure 6: Cross shelf sections of: a) potential density; b) exact geostrophic current; c) pressure gradient force error with the standard Jacobian scheme; and d) pressure gradient force error with the weighted Jacobian scheme. Horizontal resolution is 5 km and there are twenty s -levels. For the weighted Jacobian, the error is zero, but even for the standard Jacobian, the errors are generally less than 0.05% of the maximum geostrophic current.

Figure 7: As in Figure 6, but the density field is now an exponential function of depth so that the weighted Jacobian does not give the exact geostrophic current. Nevertheless, errors are generally less than 0.2% of the maximum current speed for the standard Jacobian and less than 0.02% for the weighted Jacobian. Results above 1500 m depth are shown. The horizontal distance is 200 km.

Figure 8: As in Figure 7, but the horizontal grid spacing is increased from 5 km to 20 km. Errors have risen to about 2.6% of the maximum current speeds for the standard Jacobian and to about 0.1% for the weighted Jacobian. Results above 1500 m depth are shown. The horizontal distance is 200 km.

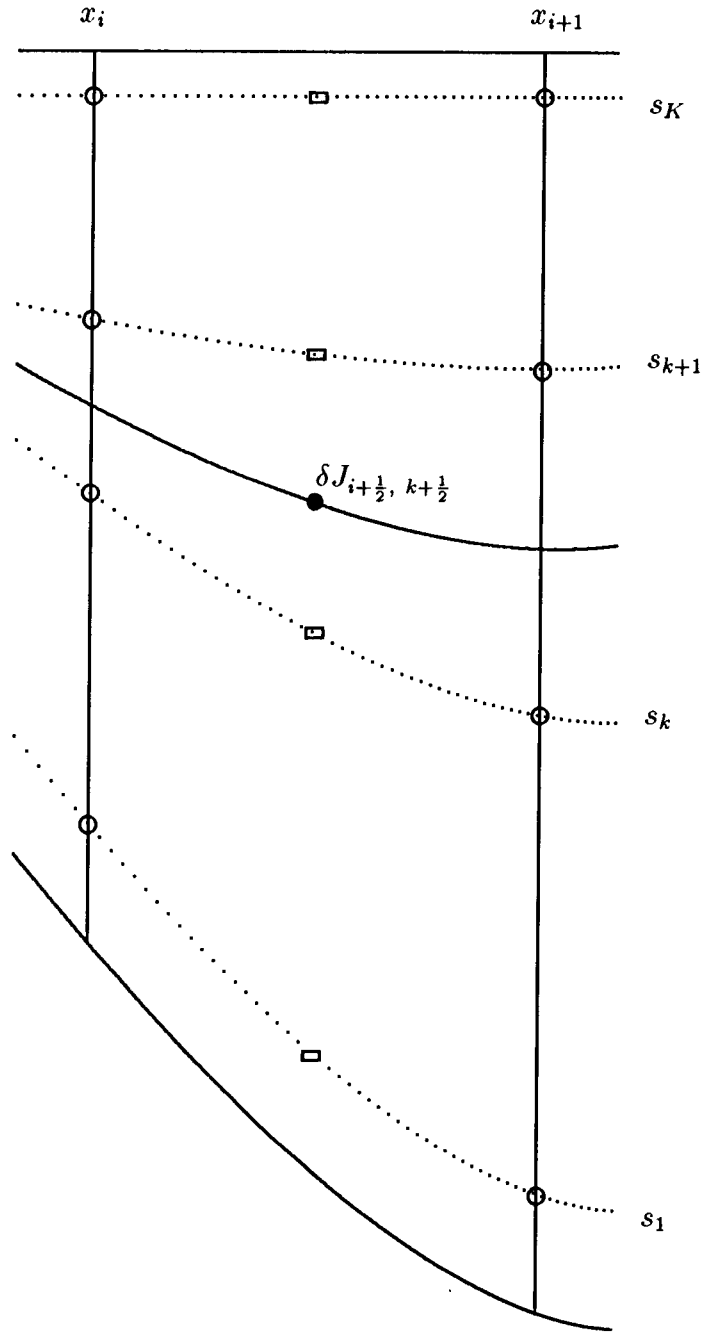


Figure 1: The computational stencil of the Arakawa C-grid in the horizontal, and a staggered grid in the vertical. The open circles are the locations of ρ and s , and the squares are the locations of u . The solid dot indicates the evaluation position for $\delta J_{i+\frac{1}{2}, k+\frac{1}{2}}$.

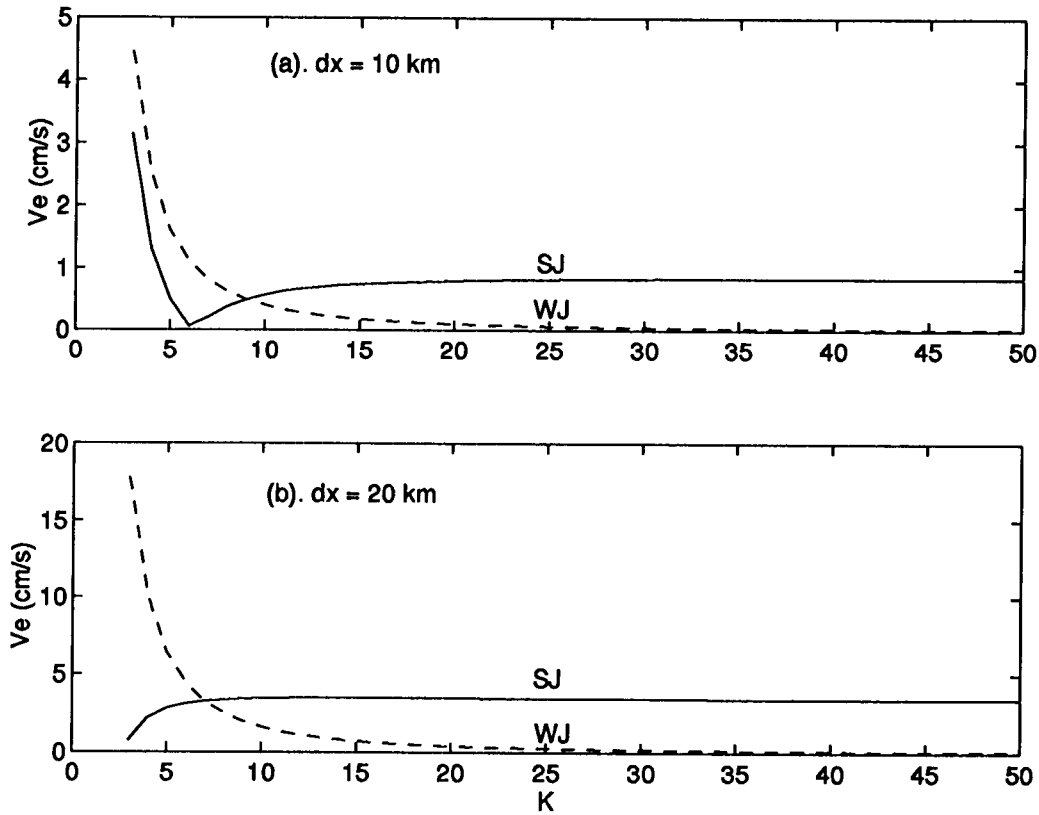


Figure 2: Theoretical estimates of the bottom level geostrophic currents caused by the pressure gradient force error as a function of the number of vertical levels (K) for a density profile which varies quadratically in the vertical. The solid lines show results predicted for the standard Jacobian and the broken lines show the results for the weighted Jacobian.

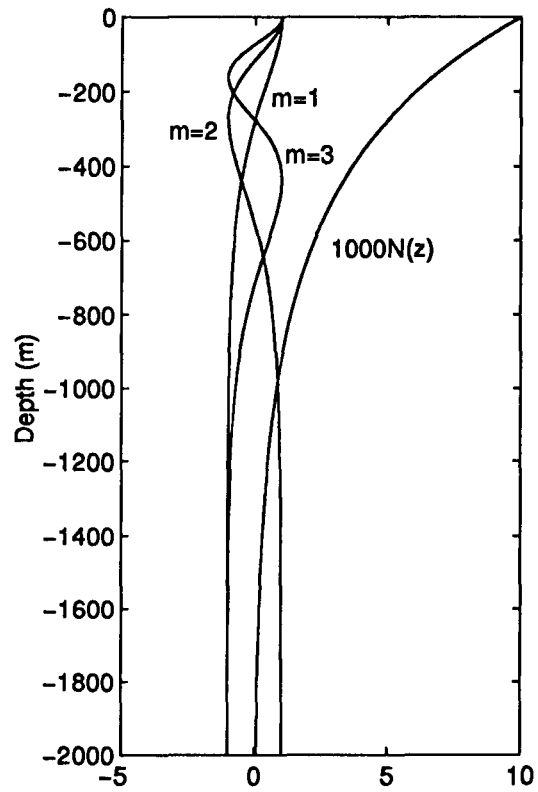


Figure 3: The vertical profiles of the buoyancy frequency ($\text{cph} \times 1000$) and the first three baroclinic Rossby modes (1°K) computed for a 2000 m deep ocean with stratification representative of the California Current region.

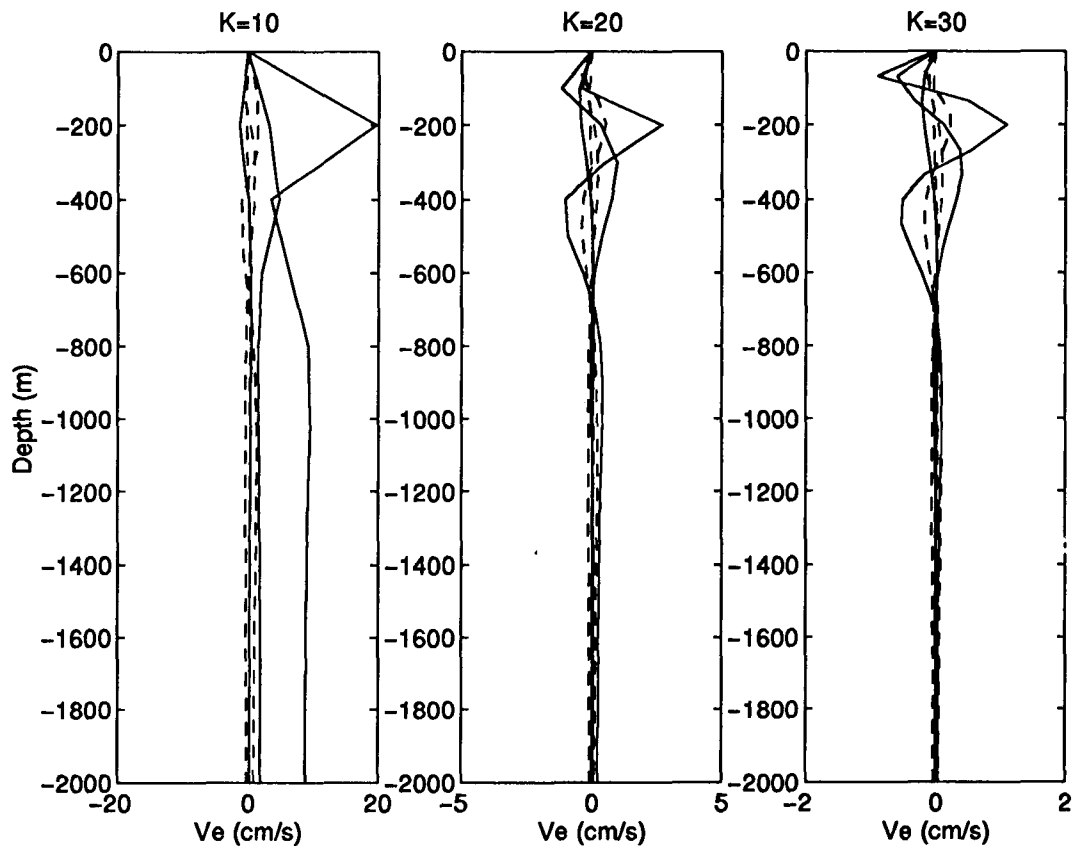


Figure 4: Vertical profiles of the pressure gradient force error using three different vertical resolutions ($K=10, 20, 30$) disturbed by the first three baroclinic Rossby modes. Solid lines indicate results computed with a uniformly spaced σ -system and dash lines correspond to results obtained with Song and Haidvogel's s -system with $\theta = 3$.

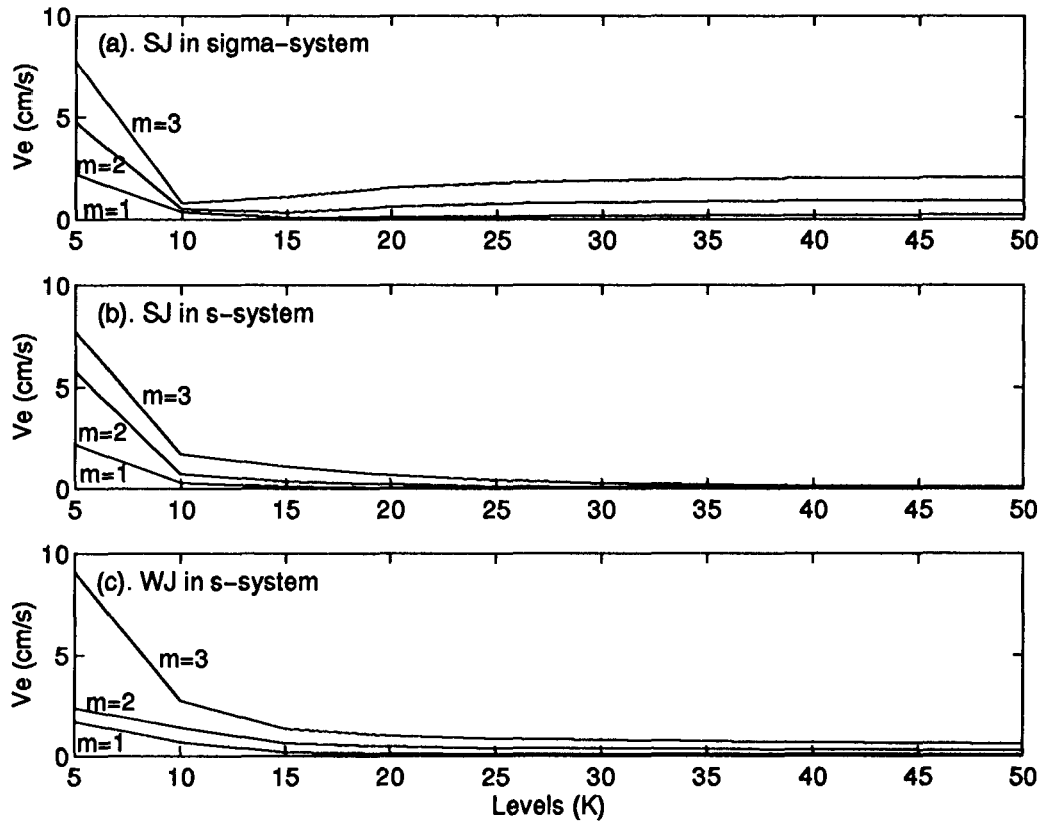


Figure 5: Maximum value of the pressure gradient error as a function of the number of vertical levels (K) for vertical density profiles corresponding to the first three Rossby wave modes. Results for the three modes are shown in each frame. The larger errors correspond to the higher modes which generally contain less of the variance under realistic conditions. The three frames show results corresponding to three different approaches: (a) the standard Jacobian scheme in σ -system; (b) the standard Jacobian scheme in the s -system with θ chosen to minimize truncation errors; (c) the weighted Jacobian scheme in the s -system with $\theta = 3$.

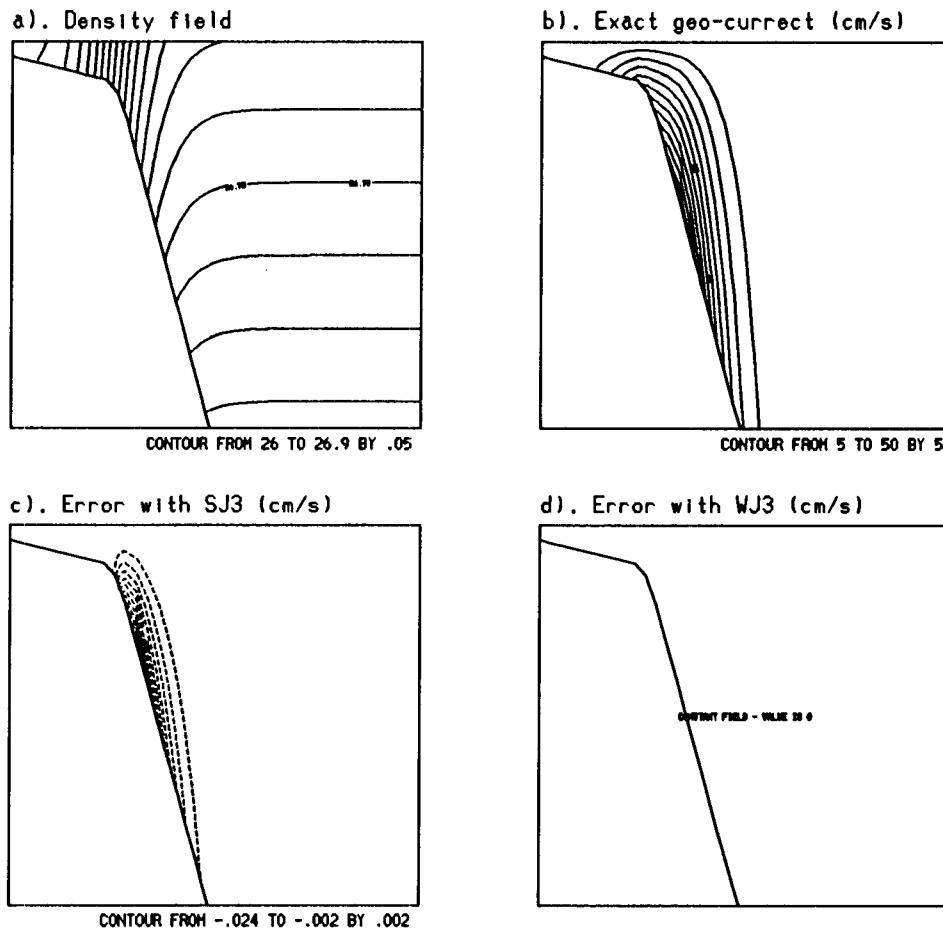


Figure 6: Cross shelf sections of: a) potential density; b) exact geostrophic current; c) pressure gradient force error with the standard Jacobian scheme; and d) pressure gradient force error with the weighted Jacobian scheme. Horizontal resolution is 5 km and there are twenty s-levels. For the weighted Jacobian, the error is zero, but even for the standard Jacobian, the errors are generally less than 0.05% of the maximum geostrophic current. Results above 1500 m depth are shown. The horizontal distance is 200 km.

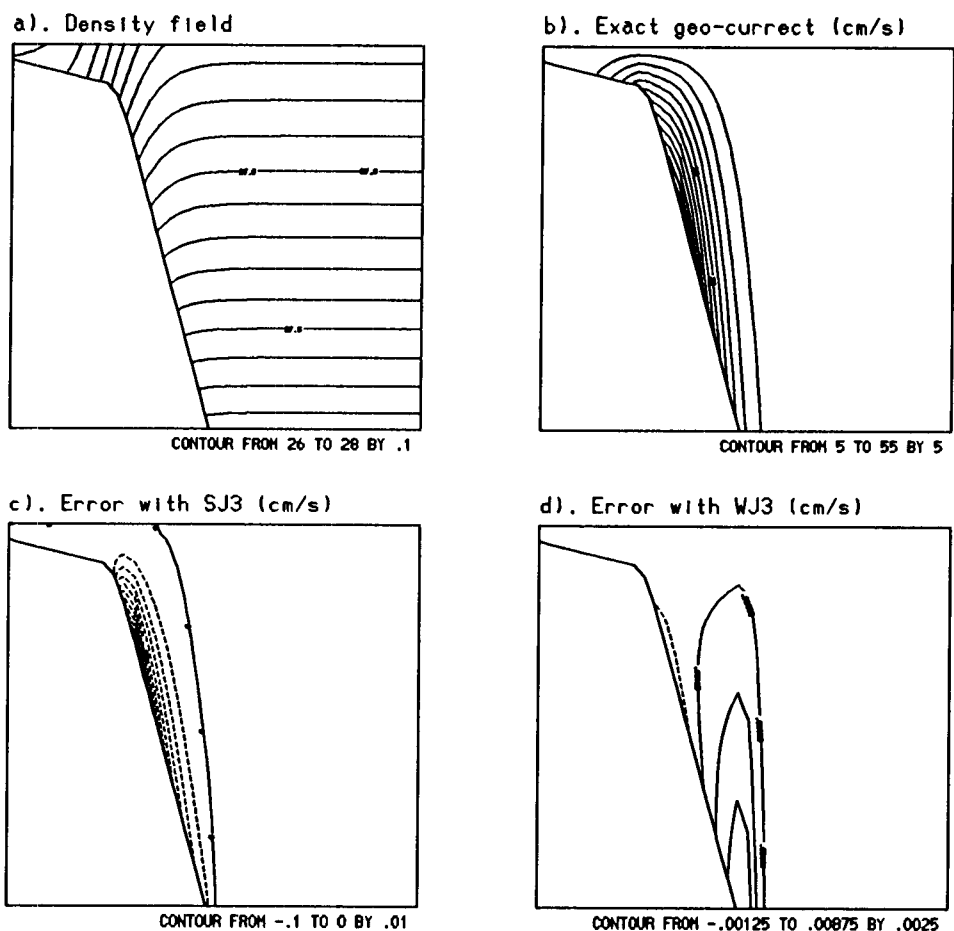


Figure 7: As in Figure 6, but the density field is now an exponential function of depth so that the weighted Jacobian does not give the exact geostrophic current. Nevertheless, errors are generally less than 0.2% of the maximum current speed for the standard Jacobian and less than 0.02% for the weighted Jacobian. Results above 1500 m depth are shown. The horizontal distance is 200 km.

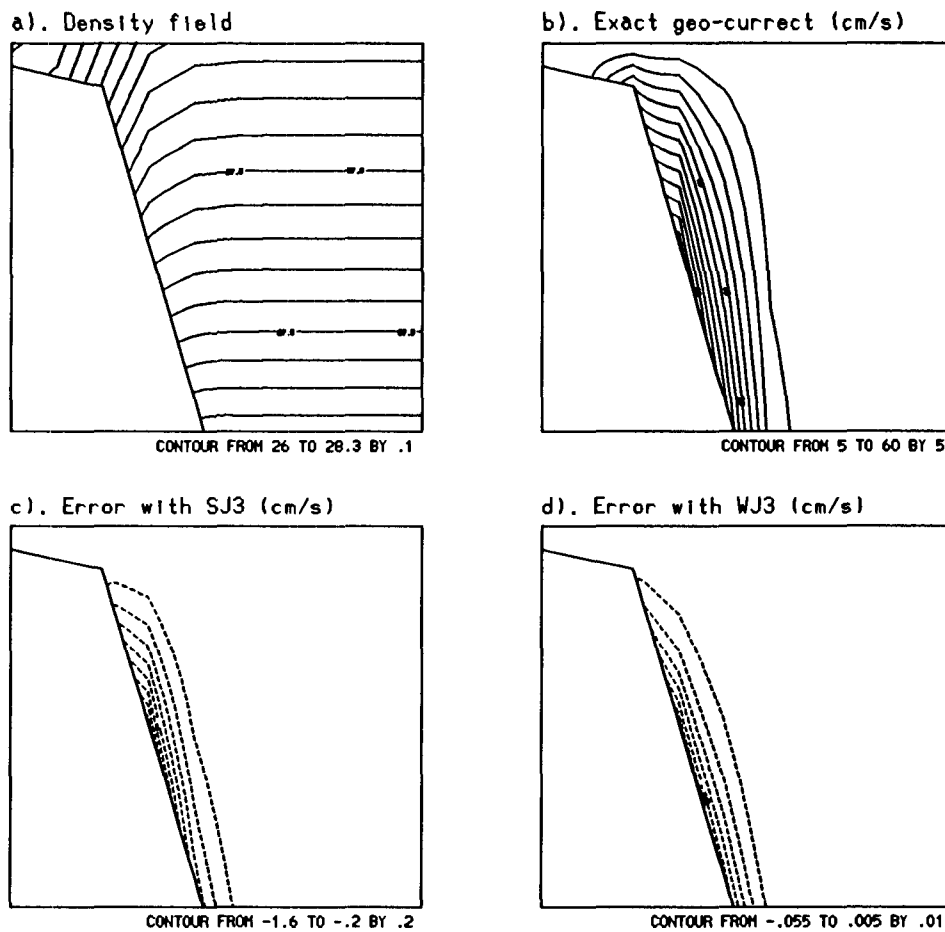


Figure 8: As in Figure 7, but the horizontal grid spacing is increased from 5 km to 20 km. Errors have risen to about 2.6% of the maximum current speeds for the standard Jacobian and to about 0.1% for the weighted Jacobian. Results above 1500 m are shown. The horizontal distance is 200 km.